J. Fluid Mech. (2023), *vol*. 977, A8, doi:10.1017/jfm.2023.941

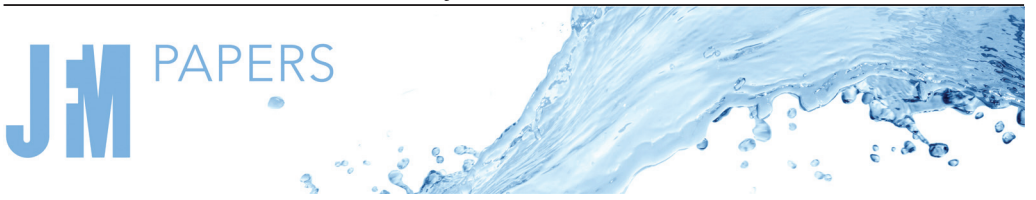

Hydrodynamics of thermally driven chiral suspensions

E. Kirkinis[1,2,†], **A.V. Andreev**[3] **and M. Olvera de la Cruz**[1,2]

[1]Department of Materials Science & Engineering, Robert R. McCormick School of Engineering and Applied Science, Northwestern University, Evanston, IL 60208, USA

[2]Center for Computation and Theory of Soft Materials, Northwestern University, Evanston, IL 60208, USA

[3]Department of Physics, University of Washington, Seattle, WA 98195, USA

(Received 18 August 2023; revised 20 October 2023; accepted 30 October 2023)

Considerable effort has been directed towards the characterization of chiral mesoscale structures, as shown in chiral protein assemblies and carbon nanotubes. Here, we establish a thermally driven hydrodynamic description for the actuation and separation of mesoscale chiral structures in a fluid medium. Cross-flow of a Newtonian liquid with a thermal gradient gives rise to an effective torque that propels each particle of a chiral suspension according to its handedness. In turn, the chiral suspension alters the liquid flow, which thus acquires a transverse (chiral) velocity component. Since observation of the predicted effects requires a low degree of sophistication, our work provides an efficient and inexpensive approach to test and calibrate chiral particle propulsion and separation strategies.

Key words: microscale transport

1. Introduction

Chirality, denoting the lack of superposition ability of structures on mirror images, is a characteristic of various assemblies, including carbon nanotubes, viruses and actin filaments, and is essential for their function. Since left- and right-handed amino acids lead to different protein structures, their homochirality is required for biological function such as gene encoding (Inaki, Liu & Matsuno 2016). Chiral proteins can sometimes lead to chiral mesoscale structures; some organisms with chiral body structures have chiral cells (Fan *et al.* 2019). Therefore, the chirality of proteins may be responsible for the chiral mesoscale structures found in cell media. Chiral mesoscale assemblies are formed in peptide amphiphiles with chiral amino acids (Gao *et al.* 2019) and in many carbon-based

† Email address for correspondence: kirkinis@northwestern.edu

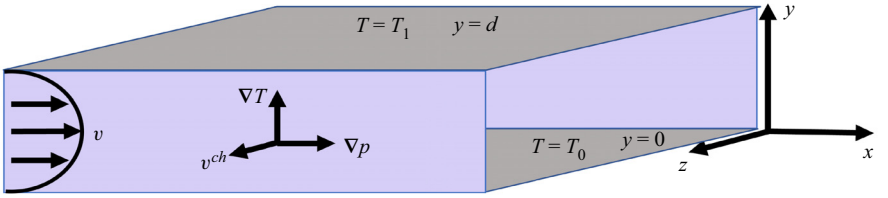

Figure 1. A chiral velocity $v^{ch}\hat{\boldsymbol{z}}$ – defined as the difference of the velocities of the left- and right-handed particles, averaged over their number density (number of particles per unit volume) – of n chiral particles suspended in a classical liquid is induced by a vertical temperature gradient $\boldsymbol{\nabla} T = \partial_y T \hat{\boldsymbol{y}}$ and shear flow $\boldsymbol{v} = u(y)\,\hat{\boldsymbol{x}}$ in a channel of width d. In a non-racemic suspension of chiral particles, the liquid is also perturbed by chirality and acquires a transverse velocity component $\delta v(y)\,\hat{\boldsymbol{z}}$ (not shown), perpendicular to the direction of the base flow $u(y)\,\hat{\boldsymbol{x}}$.

systems, which have required great efforts to understand and characterize (Arnold *et al.* 2006). However, the mechanism by which chirality manifests at the mesoscale is not well understood. Here, we propose ways of actuating and separating mesoscale chiral structures such as helices (Shimizu, Masuda & Minamikawa 2005; McCourt *et al.* 2022), helicoidal scrolls (Nagarsekar *et al.* 2016) and twisted ribbons (Oda *et al.* 1999).

The question that arises is: under what conditions can these mesoscale chiral structures propel and separate? For instance, in Andreev, Son & Spivak (2010), it was shown that in the absence of temperature gradients, chiral separation is possible only in non-stationary or nonlinear flows. However, in chemical and biological systems, various mesoscale structures move and function in an aqueous environment in the presence of thermal gradients induced by chemical reactions (Zhang *et al.* 2014). Temperature gradients may alter the liquid material parameters, and in particular viscosity, as this was demonstrated in laser-induced thermophoresis experiments (Schermer *et al.* 2011) and in associated theoretical work (Oppenheimer, Navardi & Stone 2016). In this paper, we show that the dependence of material parameters such as viscosity or density on temperature gives rise to propulsion and separation of a chiral suspension even in stationary linear flows (low Reynolds number flows). In particular, for a stationary Poiseuille flow, the segregation induced by chirality (characterized by the velocity v^{ch}) occurs in a direction normal to both the base flow and the temperature gradient; see figure 1.

Our main result is an expression for the chiral velocity $\boldsymbol{v}^{ch}$ acquired by the suspended chiral particles. The chiral velocity is defined as the difference of the velocities of the left- and right-handed particles, averaged over their number density (number of particles per unit volume). To leading order in an expansion with respect to the temperature gradient, the chiral velocity is of the form

$$\hat{\boldsymbol{z}}: \quad \langle v^{ch} \rangle = 24\chi \left(\frac{R}{d}\right)^3 U_0 \gamma\, \Delta T, \tag{1.1}$$

where ΔT is the temperature difference between the upper and lower channel walls, R is the (micron scale) chiral particle radius, d is the (millimetre scale) channel width, U_0 is a characteristic velocity scale of the base flow, $\gamma = \eta'/\eta$ is the logarithmic derivative of the viscosity, with a prime denoting differentiation with respect to temperature T, χ is a geometric scalar coefficient characteristic of the particle shape, and the brackets $\langle \cdot \rangle$ denote averaging over the channel width. Equation (1.1) is a consequence of the variation of liquid viscosity η with respect to temperature. Considerable effort has been expended in recent years in characterizing the response of active and biological liquids to

viscosity gradients (Shoele & Eastham 2018; Datt & Elfring 2019) (albeit based on the single-particle level; see the ensuing discussion).

The physical mechanism underlying the transverse chiral velocity (1.1) is the torque imparted on the base flow by the temperature gradient having the form $\boldsymbol{\nabla} T \times \nabla^2 \boldsymbol{v} + (\boldsymbol{\nabla} T \cdot \boldsymbol{\nabla})\,\mathrm{curl}\,\boldsymbol{v}$, as will be discussed in detail in § 3, where $\boldsymbol{v}$ is the velocity of the base flow, and T is its temperature. With reference to figure 1, this torque is perpendicular to both pressure and temperature gradients, thus propelling the particles along its direction.

Another aspect of the effect is that the motion of the chiral suspension in turn perturbs the base flow and endows it with a transverse velocity component δv. It is noteworthy that the chiral suspension also exerts a screw torque on the confining walls, in the direction of the base flow.

It is important to realize that the hydrodynamic description developed in this paper implies averaging over the tumbling motion of the chiral particles and applies at time scales longer than the tumbling time (Andreev *et al.* 2010). It can be understood as a 'continuum' formulation for the motion of a chiral suspension, and thus differs from the majority of propulsion descriptions that are based on a resistance matrix at the level of a single suspended particle (Happel & Brenner 1965). The equivalence of the two approaches was discussed in the recent review article by Witten & Diamant (2020).

The structure of this paper is as follows. In § 2, we describe the hydrodynamic equations of the base flow undisturbed by the chiral suspension. We have chosen an Arrhenius-type, temperature-dependent viscosity law that is valid over a large range of temperatures and is well-documented in the literature; see Fogel'son & Likhachev (2001). In § 3, we introduce the chiral current, chiral velocity v^{ch} and chiral stress following the symmetry arguments of Andreev *et al.* (2010) (derived therein when the flow is isothermal). The chiral current is the difference of the left- and right-handed particle velocities weighted by the number of particles of each handedness. The chiral velocity v^{ch} is equal to the chiral current divided by the number of particles per unit volume. Here, where non-isothermal flows are considered, one has to express the vorticity equation with respect to variations of material parameters with temperature. Our main result of the present paper appears in § 4, where we consider a suspension of chiral particles in a channel, whose base liquid is driven by crossed pressure and temperature gradients (see figure 1). Both the undisturbed by chirality flow and the chiral velocity v^{ch} can be expressed in closed form. Employing published material parameters, we estimate the magnitude of the chiral velocity and that of the liquid disturbed by chirality, henceforth denoted as δv. The main result obtained in this section is the linear dependence in ΔT of the chiral velocity v^{ch} – defined as the difference of the velocities of the left- and right-handed particles, averaged over their number density (number of particles per unit volume) – obtained for small temperature gradients. Likewise, the velocity of the liquid disturbed by chirality also depends linearly on temperature gradients ΔT. It is noteworthy that the chiral suspension exerts a screw torque on the confining walls, in the direction of the base flow. This was also observed earlier in the context of non-isothermal flows (Andreev *et al.* 2010), and here we calculate corrections due to the temperature variations. In § 5, we repeat the foregoing analysis for the practically important case of Couette flow. However, here the observables are quadratic with respect to ΔT. As in the previously considered Poiseuille flow, all observables referred to in this section are perpendicular to the base flow plane, as depicted in figure 1.

In § 6, we analyse two additional thermal effects that may give rise to non-isothermal chiral particle propulsion. The first is to consider a non-isothermal liquid, driven for

instance by a moving channel wall and endowed with viscous heating (see § 6.1), which increases the liquid temperature near the centre of the channel and thus diminishes its viscosity. The chiral velocity $\boldsymbol{v}^{ch}$ (see figure 1) depends then not on imposed temperature gradients but on the velocity scale introduced by the moving wall, and can be expressed in terms of the dimensionless Brinkman number. The second thermally related effect discussed in § 6.2 considers an alternative temperature-dependent mechanism whereby the chiral current is driven by gradients of temperature crossed with the gravitational force, in a Rayleigh–Bénard cell.

In the main body of this paper, we set the chirality parameter χ to be equal to 1. In Appendix A, we justify this choice by comparing our framework with the predictions of the single-particle theory of Makino & Doi (2004, 2017). In addition, we show that the predictions of our theory (e.g. magnitude of chiral stress) are compatible to those found in systems of similar size in biology and technology (Kataoka & Troian 1999; Ando & Yamamoto 2009).

2. Hydrodynamic equations in the absence of chirality

Conservation of entropy in an incompressible flowing liquid (Landau & Lifshitz 1987) leads to heat advection and heat conduction as well as energy dissipation due to internal friction, termed viscous heating:

$$\rho c_p(\partial_t T + \boldsymbol{v}\cdot\operatorname{grad} T) = k_{th}\,\nabla^2 T + \sigma'_{ik}\,\frac{\partial u_i}{\partial x_k}, \quad i,k=1,2,3, \tag{2.1}$$

where summation is implied on repeated indices, T is the liquid temperature, c_p is the specific heat at constant pressure, ρ is the density of the liquid, k_{th} is the thermal conductivity of the liquid, and the liquid velocity $\boldsymbol{v}$ is determined from conservation of mass and linear momentum. Also, $\sigma'_{ik} = \eta(\partial u_i/\partial x_k + \partial u_k/\partial x_i)$, $i,k=1,2,3$, is the viscous stress tensor, and η is the liquid viscosity. Rearranging the right-hand side of (2.1), one obtains

$$\rho c_p(\partial_t T + \boldsymbol{v}\cdot\operatorname{grad} T) = k_{th}\,\nabla^2 T + \frac{\eta}{2}\left(\frac{\partial u_i}{\partial x_k} + \frac{\partial u_k}{\partial x_i}\right)^2, \tag{2.2}$$

accompanied by fixed temperature boundary conditions on the vessel walls. Viscous heating can introduce hysteresis effects in Arrhenius-type viscosity laws (Davis *et al.* 1983) and affect the motion of thin liquid films (Kirkinis & Andreev 2019). In general, the viscous heating term is expected to be small and can be neglected. We will consider its effects on chiral particle propulsion in § 6.1.

Various temperature-dependent viscosity laws have been employed in the literature (see e.g. Potter & Graber 1972; Davis *et al.* 1983; Wall & Wilson 1996). Here, we will employ the well-documented Arrhenius-type temperature dependent viscosity law (Fogel'son & Likhachev 2001)

$$\eta(T) = \eta_0 \exp\left\{\frac{T_E}{T+T_A}\right\}, \quad \text{where } T_E = \frac{E}{R_g}, \tag{2.3}$$

valid in the 243–373 K temperature range, since it encompasses the linear and other exponential laws, appearing in the above references, as special cases. Here, E is the activation energy, R_g is the gas constant, and T_A is a temperature correction, unique to

Quantity	Value	Definition
η (g cm^{-1} s^{-1})	2.03	Viscosity of BM-4 oil at 25 °C (Fogel'son & Likhachev 2001)
R (cm)	5×10^{-3}	Chiral particle radius
d (cm)	0.1	Channel width
U_0 (cm s^{-1})	0.1	Poiseuille velocity
T_0 (K)	298.15	Lower channel wall temperature
γ (K^{-1})	0.07	BM-4 oil (Fogel'son & Likhachev 2001)
E (kJ mol^{-1})	7.5	Activation energy of BM-4 oil (Fogel'son & Likhachev 2001)
R_g (J mol^{-1} K^{-1})	8.31441	Gas constant
T_A (K)	−186	BM-4 oil temp. correction (Fogel'son & Likhachev 2001)
V (cm s^{-1})	1	Couette velocity
n^{ch} (cm^{-3})	R^{-3}	Chiral density $n^+ - n^-$
n (cm^{-3})	R^{-3}	Particle number density $n^+ + n^-$
u (cm s^{-1})	—	Basic shear flow velocity
v^{ch} (cm s^{-1})	—	Chiral velocity
δv (cm s^{-1})	—	Chiral correction to flow velocity

Table 1. Definitions and material parameter values (Fogel'son & Likhachev 2001).

each viscous liquid; cf. Fogel'son & Likhachev (2001) and table 1. If in a channel the lower wall $y = 0$ is kept at a temperature T_0, then linearization of (2.3) leads to

$$\eta(T) = \eta(T_0)\left[1 - \gamma(T - T_0)\right], \tag{2.4}$$

where $\gamma = E/[R_g(T_0 + T_A)^2]$ is the logarithmic derivative of the viscosity (2.3), and $\eta(T_0) = \eta_0 \exp\{E/R_g(T_0 + T_A)\}$. We will employ parameter γ in our investigations throughout this paper.

The flowing liquid satisfies the Navier–Stokes equations and is considered incompressible:

$$\rho\,(\partial_t u_i + \boldsymbol{v} \cdot \operatorname{grad} u_i) = \partial_k \sigma_{ik} \quad \text{and} \quad \partial_i u_i = 0, \tag{2.5a,b}$$

where the Cauchy stress tensor σ_{ik} is given by

$$\sigma_{ik} = -p\delta_{ik} + \eta(T)\left(\frac{\partial u_i}{\partial x_k} + \frac{\partial u_k}{\partial x_i}\right), \quad i, k = 1, 3, \tag{2.6}$$

and p is the pressure.

With a view towards understanding the structure of the vorticity equation leading to (3.8), we take the curl of both sides of (2.5a). Thus the left-hand side of (2.5a) just gives the vorticity equation for an inviscid liquid. The curl of the right-hand side of (2.5a) becomes

$$\begin{aligned}\epsilon_{ijk}\,\partial_i\partial_l\sigma_{jl} &= 2\epsilon_{ijk}\left\{\partial_i(\partial_l\eta) + (\partial_l\eta)\partial_i + (\partial_i\eta)\partial_l + \eta\,\partial_l\partial_i\right\} V_{jl} \\ &= \left\{\epsilon_{ijk}\left[\eta''\,\partial_i T\,\partial_l T + \eta'\,\partial_i\partial_l T\right] 2V_{jl} + \eta'\left[\partial_l T\,\partial_l\omega_k + \epsilon_{ijk}\,\partial_i T\,\partial_l^2 u_j\right] + \eta\,\partial_l^2\omega_k\right\},\end{aligned} \tag{2.7}$$

where a prime denotes differentiation of the viscosity η with respect to temperature T. It is clear that in the absence of nonlinear or non-stationary terms in the vorticity equation, the diffusion of vorticity is maintained in (2.7) by gradients of temperature. Also note that the linear terms in gradients of temperature in (2.7) match the terms of the chiral current introduced in (3.4).

To clarify the implications inherent in (2.7), we consider shear flow in a channel (see figure 1) whose walls are located at $y = 0, d$, for which the liquid velocity, temperature and liquid vorticity become

$$\boldsymbol{v} = u(y)\,\hat{\boldsymbol{x}}, \quad T = T(y), \quad \operatorname{curl}\boldsymbol{v} = -\partial_y u(y)\,\hat{\boldsymbol{z}} \equiv \omega\hat{\boldsymbol{z}}. \tag{2.8a–c}$$

The boundary conditions for this flow are

$$u(y=0) = u(y=d) = 0 \quad \text{and} \quad T(y=0) = T_0, \quad T(y=d) = T_1, \tag{2.9a–c}$$

where the upper channel wall is kept at a temperature $T_1 > T_0$.

For this flow, the vorticity equation becomes

$$\eta(T)\,\partial_y^2\omega = -2\eta'\left(\partial_y T\right)\partial_y\omega - \left[\eta''\left(\partial_y T\right)^2 + \eta'\,\partial_y^2 T\right]\omega, \tag{2.10}$$

by setting (2.7) equal to zero. The last term in (2.10) drops out for liquids satisfying $\partial_y^2 T = 0$ (that is, liquids whose viscous heating displayed in (2.1) is unimportant). Retaining only leading-order terms in temperature gradients, we obtain the theoretical prediction (1.1) for the chiral current.

3. Chiral current and chiral stress in non-isothermal flow

The effect that we discuss in this paper is critically dependent on the form of the chiral current, which is proportional to the chiral velocity as this was defined in the Introduction (see also (3.11) below). Thus in the ensuing paragraphs we justify the form of the chiral current on grounds of symmetry.

3.1. *Conservation of particle number*

Motion of chiral particles suspended in a classical liquid is associated with a chiral current $\boldsymbol{j}^{\pm} = n^{\pm}\boldsymbol{v}^{\pm}$, where $n^{\pm}$ are the number densities (numbers of particles per unit volume) of right- and left-handed particles, respectively, and $\boldsymbol{v}^{\pm}$ are their respective velocities. For simplicity, we consider an incompressible liquid where the right- and left-handed particles are mirror images of each other. We can thus define a chiral current $\boldsymbol{j}^{ch}$ (cf. figure 1) of the form

$$\boldsymbol{j}^{ch} = \boldsymbol{j}^{+} - \boldsymbol{j}^{-}. \tag{3.1}$$

The chiral density $n^{ch} = n^{+} - n^{-}$ satisfies the conservation law

$$\partial_t n^{ch} + \operatorname{div}(\boldsymbol{v}n^{ch}) + \operatorname{div}\left[\boldsymbol{j}(n^{ch}) + \boldsymbol{j}^{ch}\right] = 0, \tag{3.2}$$

where $\boldsymbol{j}(n) = -D\,\boldsymbol{\nabla}n - n\lambda_T\,\boldsymbol{\nabla}T - n\lambda_p\,\boldsymbol{\nabla}p$ is the particle current in the absence of chirality (Landau & Lifshitz 1987; Andreev *et al.* 2010), and $\boldsymbol{j}(n^{ch})$ is $\boldsymbol{j}(n)$ with n replaced by n^{ch}. The density $n = n^{+} + n^{-}$ of chiral particles satisfies a similar conservation equation, which is affected by chirality in a non-racemic mixture

$$\partial_t n + \operatorname{div}(\boldsymbol{v}n) + \operatorname{div}\left[\boldsymbol{j}(n) + \boldsymbol{j}^{ch}(n^{ch})\right] = 0, \tag{3.3}$$

so that (3.2) and (3.3) satisfy the Onsager principle of the symmetry of the kinetic coefficients (Landau & Lifshitz 1987).

3.2. *Chiral current*

In the presence of temperature gradients, a phenomenological expression for the chiral current $\boldsymbol{j}^{ch}$ (cf. (3.1)) based on symmetry considerations and which has a low power of derivatives of vorticity is

$$\boldsymbol{j}^{ch} = \frac{n}{T}\left[\beta_1(\boldsymbol{\nabla} T\cdot\boldsymbol{\nabla})\,\mathrm{curl}\,\boldsymbol{v} + \beta_2\,\boldsymbol{\nabla} T\times\boldsymbol{\nabla}^2\boldsymbol{v}\right], \tag{3.4}$$

where $n = n^+ + n^-$, and T, $\boldsymbol{v}$ are the liquid's, undisturbed by chirality, temperature and velocity, respectively. The coefficients β_1, β_2 will be discussed below. As mentioned above, the magnitude of the chiral current is determined by the complicated tumbling motion of the particles caused by thermal fluctuations and the inhomogeneous flow. The phenomenological expression (3.4) is written to lowest order in the driving flow. At strong drives, thermal fluctuations are subdominant, and the magnitude of the chiral current is determined by averaging over corresponding Jeffery orbits in the non-uniform flow. This problem, but in a different context, was discussed in Kirkinis, Andreev & Spivak (2012).

In Andreev *et al.* (2010), the chiral current in an isothermal system was shown to be described by the expression

$$\boldsymbol{j}^{ch} = n\beta\,\boldsymbol{\nabla}^2\mathrm{curl}\,\boldsymbol{v}. \tag{3.5}$$

Insight into the physical origin of (3.4) may be obtained by applying (3.5) to a shear flow in the presence of temperature gradients. In particular, allowing temperature dependence of the liquid viscosity η and implementing the resulting vorticity equation, (3.5) leads to

$$\boldsymbol{j}^{ch} \sim n\beta\,\frac{\eta'}{\eta}\left[\boldsymbol{\nabla} T\times\boldsymbol{\nabla}^2\boldsymbol{v} + (\boldsymbol{\nabla} T\cdot\boldsymbol{\nabla})\,\mathrm{curl}\,\boldsymbol{v}\right], \tag{3.6}$$

where a prime denotes differentiation with respect to temperature T, and we retained only leading-order terms in temperature gradients. Thus the coefficients β_1 and β_2 in (3.4) can be expressed in terms of the logarithmic derivative of viscosity with respect to temperature. We note that in the absence of temperature gradients, chiral separation is possible only in non-stationary or nonlinear flows (Andreev *et al.* 2010), as can be seen by inspection of the vorticity equation

$$\eta\,\boldsymbol{\nabla}^2\mathrm{curl}\,\boldsymbol{v} = \rho(\partial_t\mathrm{curl}\,\boldsymbol{v} + \mathrm{curl}(\boldsymbol{v}\cdot\boldsymbol{\nabla}\boldsymbol{v})), \tag{3.7}$$

and (3.5). For example, such propulsion would be present in the nonlinear pressure-driven flow induced in a convergent or divergent channel (Landau & Lifshitz 1987, § 23). In the presence of temperature gradients, however, chiral separation is possible even in the creeping flow regime. This is important for biological systems, which operate at low Reynolds numbers. This can be seen by considering a liquid whose viscosity is a function of temperature. To leading order in ΔT, the vorticity equation (3.7) is replaced by

$$\begin{aligned}\eta\,\boldsymbol{\nabla}^2\mathrm{curl}\,\boldsymbol{v} \sim{}& \eta'\left[\boldsymbol{\nabla} T\times\boldsymbol{\nabla}^2\boldsymbol{v} + (\boldsymbol{\nabla} T\cdot\boldsymbol{\nabla})\,\mathrm{curl}\,\boldsymbol{v}\right]\\ &+ \rho(\partial_t\mathrm{curl}\,\boldsymbol{v} + \mathrm{curl}(\boldsymbol{v}\cdot\boldsymbol{\nabla}\boldsymbol{v})) + O((\Delta T)^2),\end{aligned} \tag{3.8}$$

where a prime denotes differentiation with respect to temperature T. Comparison of the linear in $\boldsymbol{\nabla} T$ terms in (3.8) with (3.4) shows that the latter and (3.5) are equivalent when material parameters (here, the viscosity) vary with temperature. We note that an expression of magnetic origin for the diffusion of vorticity was also obtained in Kirkinis & Olvera de

la Cruz (2023), leading to the actuation of a suspension of chiral particles in a magnetic liquid.

When the spatial derivatives of $\boldsymbol{v}$ do not vanish, the linear in ΔT terms in (3.8) provide a scaling prediction for the magnitude of the chiral current (3.5), and equivalently for the chiral velocity v^{ch} in the form (1.1). This is a main consequence of the symmetries leading to (3.4), and will be derived explicitly in § 4.

3.3. *Chiral stress*

A chiral suspension imparts stresses on the suspending liquid. To leading order in velocity gradients, these stresses, allowed by symmetry, read

$$\sigma_{ij}^{ch} = \eta(T)\, n^{ch} \left\{ \alpha \left[\partial_i (\mathrm{curl}\, \boldsymbol{v})_j + \partial_j (\mathrm{curl}\, \boldsymbol{v})_i \right] + \frac{\alpha_1}{T} \left[\epsilon_{kli} V_{kj} + \epsilon_{klj} V_{ki} \right] \partial_l T \right\}, \tag{3.9}$$

where V_{ij} is the rate-of-strain tensor. The first square bracket term of (3.9) introduced in Andreev *et al.* (2010) was discussed in the recent review Witten & Diamant (2020). The second square bracket term exists only when temperature gradients are present in the liquid.

The coefficients β, α and α_1 in (3.5) and (3.9) are determined in the low Reynolds number regime by studying the particle motion in the surrounding liquid (Happel & Brenner 1965). They may be estimated as

$$\alpha \sim \alpha_1 \sim \chi R^4 \quad \text{and} \quad \beta \sim \chi R^3, \tag{3.10a,b}$$

where R is the chiral particle radius, and χ is the degree of chirality in the shape of the particles. Equations (3.10*a*,*b*) provide the order of magnitude estimates of these coefficients. Their precise determination for a specific particle shape, however, requires solving hydrodynamic equations for a tumbling particle in the presence of temperature and velocity gradients, and is beyond the scope of our work. For simplicity, we consider an incompressible liquid where the right- and left-handed particles are mirror images of each other.

3.4. *Chiral velocity*

The programme to be followed in this paper is as follows. First, we will determine the form of the base flow, undisturbed by chirality, and denoted by $\boldsymbol{v} = u(y)\,\hat{\boldsymbol{x}}$ with reference to figure 1. From this, we calculate the chiral velocity v^{ch} as

$$\boldsymbol{v}^{ch} \equiv \boldsymbol{j}^{ch}/n, \tag{3.11}$$

which, through (3.5), gives rise to the main observable, that is, the chiral current $\boldsymbol{j}^{ch}$. We calculate explicitly the stresses imparted on the liquid and on the two channel walls by the chiral stress (3.9). The Cauchy stress tensor in (2.6) thus needs to be updated by the chiral contribution (3.9) to take into account the effects of the chiral suspension on the base liquid. Thus we calculate explicitly the chiral suspension-induced perturbation δv of the liquid base flow.

4. Chiral particle separation in crossed pressure and temperature gradients

4.1. *Non-isothermal base Poiseuille flow (without chiral particles)*

Consider pressure-driven flow in a channel with uneven heated walls (cf. figure 1). With $\boldsymbol{v} = u(y)\,\hat{\boldsymbol{x}}$, $\nabla T = \partial_y T \hat{\boldsymbol{y}}$, the Navier–Stokes equations (2.5*a*,*b*) and energy balance (2.2) in

the creeping flow approximation reduce to

$$\frac{\mathrm{d}}{\mathrm{d}y}\left[\eta(T)\,\frac{\mathrm{d}u}{\mathrm{d}y}\right]=\frac{\mathrm{d}p}{\mathrm{d}x},\quad \frac{\mathrm{d}^2T}{\mathrm{d}y^2}=0, \tag{4.1a,b}$$

respectively, with boundary conditions

$$u(0)=u(d)=0,\quad T(0)=T_0,\quad T(d)=T_0+\Delta T. \tag{4.2a–c}$$

The energy equation temperature profile thus obtained is $T(y)=T_0+(y/d)\,\Delta T$. Let

$$X_i=\frac{T_E}{T_A+T_i},\quad i=0,1,2,\quad \text{and}\quad T_E=\frac{E}{R_g}, \tag{4.3a,b}$$

where T_0 and $T_1=T_0+\Delta T$ are the lower and upper wall fixed temperatures, respectively, $T_2\equiv T=T_0+(y/d)\,\Delta T$, and E, R_g and T_A are the activation energy, gas constant and correction temperature as defined in table 1, respectively. The solution of the first equation of (4.1*a*,*b*) with boundary conditions (4.2*a–c*) becomes

$$u=\frac{T_E^2 d^2\,\partial_x p}{2\eta(T)\,(\Delta T)^2}\,\frac{\displaystyle\sum_{\{i,j,k\}}\mathrm{e}^{X_i}\left\{Ei_1(X_i)\left[\frac{\mathrm{e}^{X_j}}{X_k^2}-\frac{\mathrm{e}^{X_k}}{X_j^2}\right]+\frac{1}{X_jX_k}\left(\frac{1}{X_k}-\frac{1}{X_j}\right)\right\}}{[Ei_1(X_0)-Ei_1(X_1)]\,\mathrm{e}^{X_0+X_1}+\dfrac{\mathrm{e}^{X_0}}{X_1}-\dfrac{\mathrm{e}^{X_1}}{X_0}}, \tag{4.4}$$

where the y dependence arises through $X_2(T(y))$ (see (4.3*a*,*b*)), the symbol $\{i,j,k\}$ means cyclic permutation of i, j and k, and

$$Ei_1(X)=\int_1^\infty\frac{\mathrm{e}^{-kX}}{k}\,\mathrm{d}k \tag{4.5}$$

is the exponential integral.

4.2. *Chiral velocity*

Now consider the presence of chiral particles and define the chiral velocity (3.11), $\boldsymbol{v}^{ch}\equiv\boldsymbol{j}^{ch}/n$, relative to the liquid by employing (3.5). With respect to the geometry displayed in figure 1, it has the form $\boldsymbol{v}^{ch}=v^{ch}(y)\,\hat{\boldsymbol{z}}$, and its magnitude is

$$v^{ch}=\chi\,\frac{R^3}{d}\,\frac{X_2^4\,\Delta T\,\partial_x p}{2\eta(T)\,T_E}\times\frac{[Ei_1(X_1)-Ei_1(X_0)]\,\mathrm{e}^{X_0+X_1}+\displaystyle\sum_{i\,\neq j=0,1}\frac{(-1)^i\mathrm{e}^{X_j}}{X_i^2}\left[\frac{1}{2}+\frac{1}{X_i}\left(\frac{1}{X_2}-\frac{1}{2}\right)\right]}{[Ei_1(X_0)-Ei_1(X_1)]\,\mathrm{e}^{X_0+X_1}+\dfrac{\mathrm{e}^{X_0}}{X_1}-\dfrac{\mathrm{e}^{X_1}}{X_0}}, \tag{4.6}$$

where the y-dependence again arises through $X_2(T(y))$ (see (4.3*a*,*b*)). In figure 2, we plot the closed-form expression (4.6) for the chiral velocity δv in cm s^{-1} versus channel elevation y in cm for two temperature variations ΔT between the lower (at $y=0$) and upper (at $y=0.1$ cm) channel walls. As can be seen in figure 2, velocity proliferation is favoured near the upper heated wall where viscosity is diminished. In addition, particle velocities

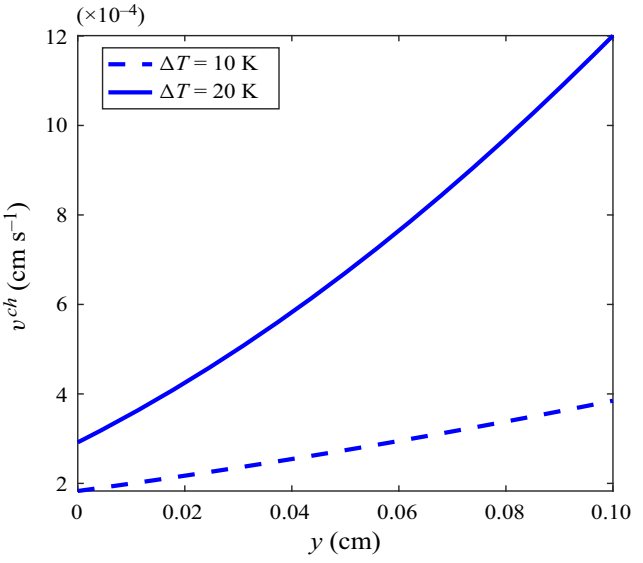

Figure 2. Chiral particle velocity v^{ch} in cm s^{-1} from (4.6), perpendicular to the x–y plane formed by a base Poiseuille flow and the vertical temperature gradient directions (cf. figure 1). Here, y is the vertical channel coordinate in cm, and we employed the Arrhenius-type temperature dependent viscosity law (2.3) for a BM-4 oil (Fogel'son & Likhachev 2001). We have set $\chi = 1$ (see the discussion in Appendix A).

are non-zero close to the solid walls located at $y = 0, d$, even though no-slip boundary conditions are satisfied by the base liquid. This is the case because, according to (3.5), chiral particle velocities become prominent in the vicinity of large vorticity gradients, and these are present close to solid walls.

Relation (4.6) is tidy but uninformative. To obtain an understanding of the effect, we average (4.6) over the channel width d, and expand with respect to ΔT to obtain $\langle v^{ch}\rangle \sim 2\chi R^3\gamma(\Delta T/d)(\partial_x p/\eta)$, to leading order in ΔT, where we defined the average of a function $f(y)$ with respect to the channel width to be $\langle f\rangle = (1/d)\int_0^d f(y)\,\mathrm{d}y$, R is chiral particle size, d is channel width, and γ is the logarithmic derivative of viscosity; see the discussion below (2.4). It is more illuminating, however, to replace the pressure gradient with a characteristic velocity U_0 of Poiseuille flow by averaging the (undisturbed by chirality) base Poiseuille profile $u \sim \partial_x p/2\eta(T_0)\,(y^2 - yd)$ over the channel width d. This gives $U_0 = -(\partial_x p/12\eta(T_0))d^2$, and substituting into the expression for $\langle v^{ch}\rangle$, we obtain the single-particle velocity

$$\langle v^{ch}\rangle = 24\chi\left(\frac{R}{d}\right)^3 U_0\gamma\,\Delta T. \tag{4.7}$$

Considering BM-4 oil (Fogel'son & Likhachev 2001), $\Delta T = 10$ K and the values displayed in table 1, (4.7) leads to the estimate

$$v^{ch} \sim 2\chi\ \mu\mathrm{m\ s}^{-1}. \tag{4.8}$$

The Reynolds number is $Re \sim 3.4 \times 10^{-3}$. Analogous results can be derived for silicon oils employed in the experiments of Ehrhard (1993) and other liquids reported in the literature (Fogel'son & Likhachev 2001). Water can also be used, although it leads to Reynolds numbers higher than those reported here.

4.3. *Perturbation of liquid velocity by the chiral suspension*

A chiral suspension imparts stresses on the suspending liquid. To leading order in gradients of vorticity, these stresses, allowed by symmetry, are given by (3.9)). Here, $n^{ch} = n^+ - n^-$ is the chiral density, and n^+ and n^- are the number densities of right- and left-handed particles, respectively. Thus the liquid velocity $\boldsymbol{v}$ acquires a chirality-induced component δv perpendicular to the plane of the flow:

$$\boldsymbol{v} = u(y)\,\hat{\boldsymbol{x}} + \delta v(y)\,\hat{\boldsymbol{z}}. \tag{4.9}$$

With the chiral correction (3.9), the Cauchy stress tensor reads

$$\sigma_{ij} = -p\delta_{ij} + \eta(\partial_i u_j + \partial_j u_i) + \sigma_{ij}^{ch}. \tag{4.10}$$

Conservation of linear momentum $\partial_j \sigma_{ij} = 0$ along the flow direction $\hat{\boldsymbol{x}}$: $-\partial_x p + \partial_y(\eta\,\partial_y u) = 0$ is now accompanied by its chirality-induced counterpart that is perpendicular to the base flow direction,

$$\hat{\boldsymbol{z}}\colon \partial_y(\eta\,\partial_y \delta v) - n^{ch}\chi R^4\,\partial_y(\eta\,\partial_y^2 u) = 0, \tag{4.11}$$

and satisfies no-slip boundary conditions

$$\delta v(0) = \delta v(d) = 0. \tag{4.12}$$

The solution δv of (4.11) with boundary conditions (4.12) is displayed in figure 3 in cm s^{-1} versus channel elevation y in cm for two temperature variations ΔT between the lower (at $y = 0$) and upper (at $y = 0.1$ cm) channel walls, employing the Arrhenius-type temperature-dependent viscosity law (2.3). Its profile is skewed due to the reduction of viscosity close to the upper heated channel wall, which is also the location of high chiral velocity v^{ch}.

To leading order in ΔT, and averaging over the channel width d, we obtain $\delta v \sim \chi R(d\,\partial_x p/12\eta)\gamma\,\Delta T$. Replacing the pressure gradient with its Poiseuille flow counterpart leads to

$$\delta v \sim \chi\,\frac{R}{d}\,U_0\gamma\,\Delta T. \tag{4.13}$$

Employing the material parameters for BM-4 oil displayed in table 1, and setting $\Delta T =$ 10 K, we obtain the estimate

$$\delta v \sim 35\chi\ \mu\text{m s}^{-1}, \tag{4.14}$$

which agrees well, in order of magnitude, with the exact solution displayed in figure 3. The momentum equation displayed in (4.11) was formulated by considering only the first term of the constitutive law (3.9), since the second term – for the material parameters employed in this paper – gives velocities that are one order of magnitude smaller than the ones derived here.

4.4. *Screw torque in a non-racemic suspension*

A non-racemic mixture will apply shear stresses on the channel walls that are perpendicular to the plane of the paper. These forces arise from the chiral momentum

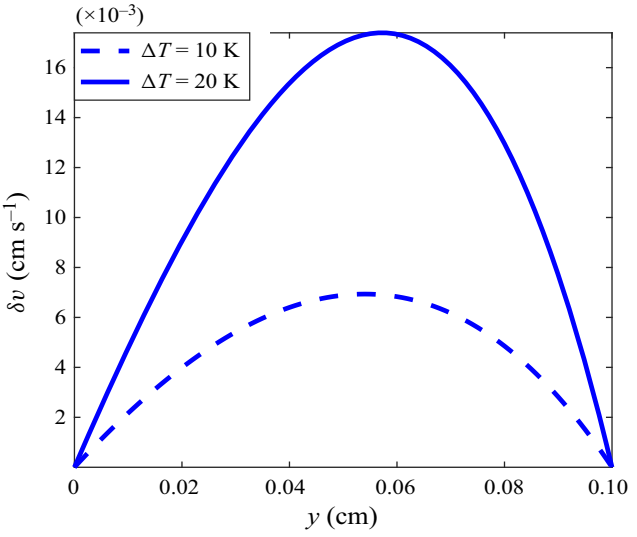

Figure 3. Transverse chiral component of liquid velocity δv in cm s^{-1}, perpendicular to the x–y plane formed by a Poiseuille flow and the temperature gradient directions (cf. figure 1) and obtained by solution of (4.11) with boundary conditions (4.12). Here, y is the vertical channel coordinate in cm, and we employed the Arrhenius-type temperature dependent viscosity law (2.3) for a BM-4 oil (Fogel'son & Likhachev 2001), giving rise to the skewness of chiral velocity profiles. We have set $\chi = 1$ (see the discussion in Appendix A).

flux density (3.9) (Andreev *et al.* 2010). Employing the geometry of the channel Poiseuille flow displayed in figure 1, this stress is of the form

$$\sigma_{zy}^{ch} = \chi R \eta \, \partial_y^2 u. \tag{4.15}$$

In figure 4, we display the chiral stress σ_{zy}^{ch} as a function of channel width employing the exact form for the liquid velocity profile (4.4). Since the normal vectors to the two channel walls have opposite sign, the chiral suspension exerts on the walls two forces of opposite sign directed into and out of the page. Hence there is a screw torque exerted by the chiral flow on the confining walls, directed along the flow.

Calculating the average of the chiral stress $\langle \sigma_{zy}^{ch} \rangle$ over the channel width, and expanding with respect to ΔT, we obtain

$$\langle \sigma_{zy}^{ch} \rangle = \chi R \, \partial_x p (1 + \tfrac{1}{2} \gamma \, \Delta T) + O((\Delta T)^2). \tag{4.16}$$

Expression (4.16) implies that a chiral stress exists even in the absence of temperature gradients. This was also noted in Andreev *et al.* (2010). Replacing the pressure gradient by the base Poiseuille profile, as carried out in the foregoing sections and employing the material values appearing in table 1 for $\Delta T = 10$ K, (4.16) gives

$$\langle \sigma_{zy}^{ch} \rangle = 1.21 \chi (1 + 0.43) + O((\Delta T)^2) \text{ dynes cm}^{-2}. \tag{4.17}$$

Doubling ΔT, one needs to double only the number 0.43 in this last expression.

5. Non-isothermal chiral separation and propulsion in Couette flow

The practically important case of Couette flow under a vertical temperature gradient in a channel whose upper wall slides with velocity V also gives a commensurate chiral particle

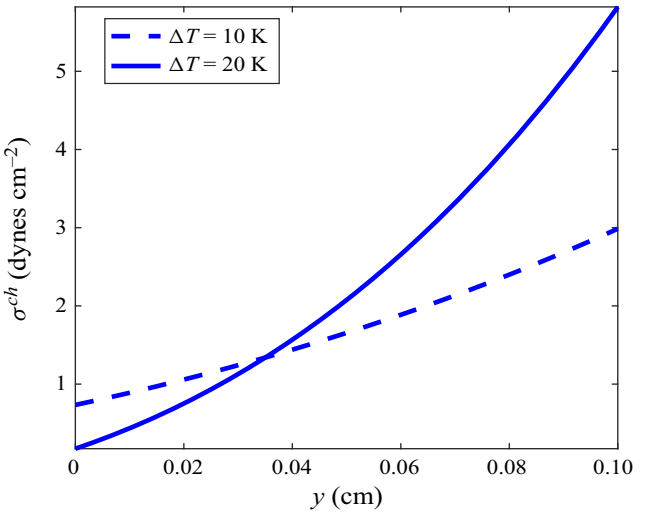

Figure 4. Distribution of the chiral stress σ_{zy}^{ch} in (4.15) in dynes cm^{-2} imparted by the chiral suspension on the liquid in a direction perpendicular to the x–y plane formed by the Poiseuille flow and the vertical temperature gradient (cf. figure 1), versus the vertical coordinate y of the channel in cm. We employed the Arrhenius-type temperature-dependent viscosity law (2.3) for a BM-4 oil (Fogel'son & Likhachev 2001). Since the normal vectors to the two channel walls have opposite sign, the chiral suspension exerts on the walls two forces of opposite sign directed into and out of the page. Hence there is a screw torque exerted by the chiral flow on the confining walls, directed along the base flow direction. We have set $\chi = 1$ (see the discussion in Appendix A).

propulsion: $\boldsymbol{v} = u(y)\,\hat{\boldsymbol{x}}$, $\boldsymbol{\nabla} T = \partial_y T \hat{\boldsymbol{y}}$. In this case, the Navier–Stokes and energy balance equations in the creeping flow approximation reduce to

$$\frac{\mathrm{d}}{\mathrm{d}y}\left[\eta(T)\,\frac{\mathrm{d}u}{\mathrm{d}y}\right] = 0, \quad \frac{\mathrm{d}^2 T}{\mathrm{d}y^2} = 0, \tag{5.1a,b}$$

with boundary conditions

$$u(0) = 0, \quad u(d) = V, \quad T(0) = T_0, \quad T(d) = T_1 \equiv T_0 + \Delta T. \tag{5.2a–d}$$

The energy equation temperature profile thus obtained is $T(y) = T_0 + (y/d)\,\Delta T$.

The vorticity equation in the form (2.10) still holds, but because of the form of the Couette flow profile, contributions on the right-hand side of (2.10) will all be of second order in ΔT. Employing the notation introduced in (4.3a,b), the chiral separation velocity takes the form

$$v^{ch} = \chi R^3\,\frac{V}{d^3}\,\frac{X_2^4\left(\dfrac{1}{X_0}-\dfrac{1}{X_1}\right)^3\left(\dfrac{2}{X_2}-1\right)\mathrm{e}^{X_0+X_1-X_2}}{[Ei_1(X_0)-Ei_1(X_1)]\,\mathrm{e}^{X_0+X_1}+\dfrac{\mathrm{e}^{X_0}}{X_1}-\dfrac{\mathrm{e}^{X_1}}{X_0}}. \tag{5.3}$$

In figure 5, we plot the closed-form expression (5.3) for the individual particle velocity v^{ch} in cm s^{-1} versus channel elevation y in cm for two temperature variations ΔT between the lower (at $y = 0$) and upper (at $y = 0.1$ cm) channel walls.

Averaging (5.3) over the channel width d, and expanding with respect to ΔT, we obtain the chiral separation velocities $\langle v^{ch}\rangle$, which are now quadratic with respect to the

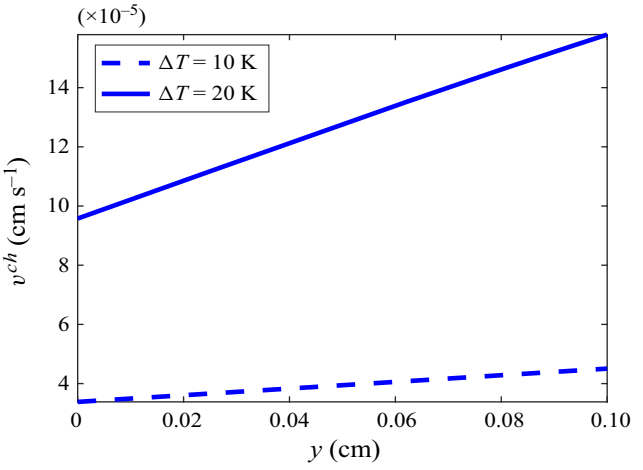

Figure 5. Chiral particle velocity v^{ch} in cm s^{-1} from (5.3), perpendicular to the x–y plane formed by the Couette flow and temperature gradient directions (cf. figure 1). Here, y is the vertical channel coordinate in cm, and we employed the Arrhenius-type temperature-dependent viscosity law (2.3) for a BM-4 oil (Fogel'son & Likhachev 2001). The base flow is generated by the motion of the upper channel wall with velocity 1 cm s^{-1}. We have set $\chi = 1$ (see the discussion in Appendix A).

temperature gradient strength ΔT:

$$\langle v^{ch} \rangle \sim 2\chi V \left(\frac{R}{d}\right)^3 \frac{T_A + T_0 - \dfrac{T_E}{2}}{(T_A + T_0)^4} T_E (\Delta T)^2 \tag{5.4}$$

(see table 1 for the meaning of the various temperature scales). Considering the parameter values displayed in table 1, upper channel wall velocity $V = 1$ cm s^{-1} and $\Delta T = 10$ K, we obtain

$$\langle v^{ch} \rangle \sim 0.483 \ \mu\text{m s}^{-1}, \tag{5.5}$$

which agrees well with the corresponding curve of figure 5. The Reynolds number is $Re \sim 3.4 \times 10^{-2}$. In a manner analogous to the pressure-driven flow of § 4, the suspension will give rise to a transverse chiral component of liquid velocity v^{ch} perpendicular to the plane of the flow, also calculated for an upper wall velocity 1 cm s^{-1} employing the nonlinear Arrhenius viscosity law (2.3) by solving for δv in (4.11) with boundary conditions (4.12) when the base flow is given by the Couette profile obtained from (5.1*a*,*b*) and (5.2*a*–*d*). The liquid transverse chiral velocity δv obtained in this manner is displayed in figure 6.

6. Related thermal effects

6.1. *Viscous heating-induced chiral particle propulsion*

We note the existence of two rather special related thermal effects for the propulsion of chiral particles. The first concerns the effects of viscous heating in the interior of a channel when the viscosity is temperature-dependent and thermal gradients are generated at the interior by viscous heating (Kirkinis & Andreev 2019). Referring to the geometry displayed in figure 1, where $\boldsymbol{v} = u(y)\,\hat{\boldsymbol{x}}$, $\nabla T = \partial_y T \hat{\boldsymbol{y}}$ (here, however, the two walls are kept at equal temperatures), one can follow the formulation of this problem developed by Davis

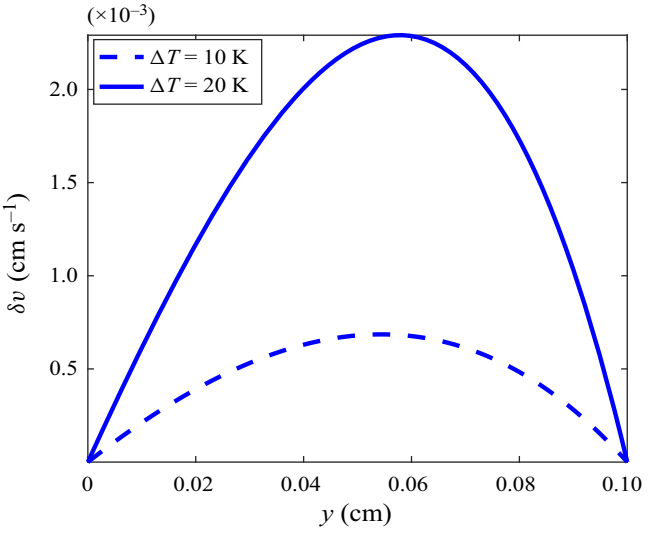

Figure 6. Transverse chiral component of liquid velocity δv in cm s^{-1}, perpendicular to the x–y plane formed by the Couette flow and temperature gradient directions (cf. figure 1) by solving for δv in (4.11) with boundary conditions (4.12), when the base flow is given by the Couette profile obtained from (5.1*a*,*b*) and (5.2*a*–*d*). Here, y is the vertical channel coordinate in cm, and we employed the Arrhenius-type temperature-dependent viscosity law (2.3) for a BM-4 oil (Fogel'son & Likhachev 2001), giving rise to the skewness of the chiral velocity profiles. The base flow is generated by the motion of the upper channel wall with velocity 1 cm s^{-1}. We have set $\chi = 1$ (see the discussion in Appendix A).

et al. (1983):

$$\frac{\mathrm{d}}{\mathrm{d}y}\left[\eta(T)\,\frac{\mathrm{d}u}{\mathrm{d}y}\right] = 0, \quad k_{th}\,\frac{\mathrm{d}^2T}{\mathrm{d}y^2} + \eta\left(\frac{\mathrm{d}u}{\mathrm{d}y}\right)^2 = 0, \tag{6.1a,b}$$

with boundary conditions

$$u(0) = 0, \quad u(d) = V, \quad T(0) = T(d) = T_0. \tag{6.2a–c}$$

Employing the Arrhenius law, the problem can be solved only numerically. The interest here would be the effect of hysteresis present between the shear rate and shear stress, as this was studied in detail by Davis *et al.* (1983). When $|T - T_0|/T_0 < 1$, a valid approximation to the Arrhenius law given as $\eta(T) = \eta_0 \exp(-\gamma(T - T_0))$ and the solution of (6.1*a*,*b*) with boundary conditions (6.2*a*–*c*) can be obtained in closed form. The effect is quantified by the Brinkman number

$$Br = \frac{\gamma \eta_0 V^2}{k_{th}}, \tag{6.3}$$

where γ is the logarithmic derivative of the viscosity defined in (2.4). Exact expressions for the particle velocity and temperature are then (Gavis & Laurence 1968; Sukanek, Goldstein & Laurence 1973)

$$u = \frac{V}{2}\left(1 + c\tanh b\left(2\,\frac{y}{d} - 1\right)\right) \quad \text{and} \quad \gamma(T - T_0) = \ln\left(a\,\mathrm{sech}^2 b\left(2\,\frac{y}{d} - 1\right)\right), \tag{6.4a,b}$$

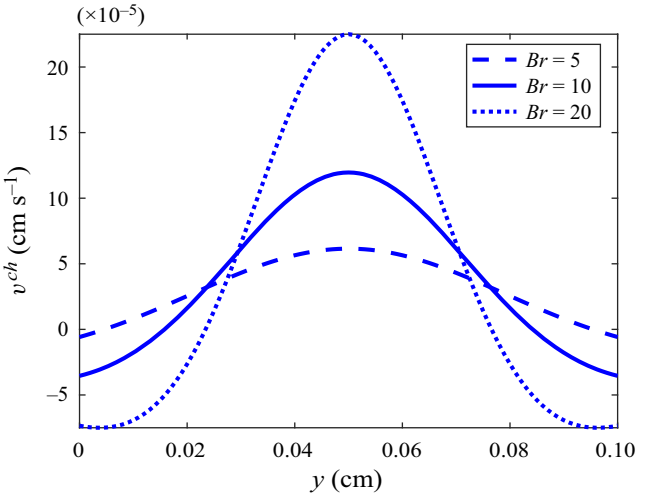

Figure 7. Chiral particle velocity v^{ch} in cm s^{-1} from (6.6), perpendicular to the x–y plane formed by the motion of the upper wall with velocity $V = 0.1$ cm s^{-1}. Most of the propulsion is generated at the interior, which is the location of increased temperature gradients due to viscous heating and thus of diminishing liquid viscosity. We have set $\chi = 1$ (see the discussion in Appendix A).

where

$$a = 1 + \tfrac{1}{8}\,Br, \quad b = \sinh^{-1}\left(\tfrac{1}{8}\,Br\right)^{1/2} \quad \text{and} \quad c = \left(\frac{1+\dfrac{1}{8}\,Br}{\dfrac{1}{8}\,Br}\right)^{1/2}. \tag{6.5a–c}$$

It is thus easy to calculate the chiral velocity v^{ch} in the form

$$v^{ch} = -\chi V \left(\frac{R}{d}\right)^3 \frac{32 b^3 c \left(-2 + \cosh\left(\dfrac{(-4y+2d)\,b}{d}\right)\right)}{\left(\cosh\left(\dfrac{(-4y+2d)\,b}{d}\right)+1\right)^2}. \tag{6.6}$$

Figure 7 displays three representative chiral velocity curves within the channel of width 0.1 cm employing the exact expression (6.6). Viscous heating and diminishing of the liquid viscosity near the channel centre lead to increased particle velocities. For very high Brinkman numbers, the profiles display additional maxima at the interior.

Averaging (6.6) over the width of the channel, and expanding for small Br, we obtain

$$\langle v^{ch} \rangle = \chi \left(\frac{R}{d}\right)^3 V\, Br \left(1 - \frac{1}{6}\,Br + O(Br^2)\right). \tag{6.7}$$

For $Br = 0.8$, $d = 0.1$ cm and $V = 0.1$ cm s^{-1}, we find

$$\langle v^{ch} \rangle = 0.1\ \mu\text{m s}^{-1}. \tag{6.8}$$

6.2. *Rayleigh–Bénard convection-induced chiral particle propulsion*

Another related thermally induced chiral particle propulsion effect can take place in a Rayleigh–Bénard cell (Chandrasekhar 1961), driven by variations of the liquid density with temperature (thus the viscosity is considered to be a constant in this subsection). Here, the coefficient of thermal expansion α_T is the logarithmic derivative of density with respect to temperature, in the same sense that γ in (2.4) is the logarithmic derivative of viscosity. Diffusion of vorticity, perpendicular to the plane of the cell, is now expressed in the form

$$\eta\,\nabla^2 \mathrm{curl}\,\boldsymbol{v} = \rho_0 \alpha_T \boldsymbol{g} \times \boldsymbol{\nabla} T + \rho_0(\partial_t \mathrm{curl}\,\boldsymbol{v} + \mathrm{curl}(\boldsymbol{v}\cdot\boldsymbol{\nabla}\boldsymbol{v})), \tag{6.9}$$

where $\boldsymbol{g}$ is the gravitational acceleration, $\rho = \rho_0[1 - \alpha_T(T - T_0)]$, $\rho = \rho_0$ at $T = T_0$, and $\alpha_T \equiv -(1/\rho)(\partial\rho/\partial T) > 0$ is the coefficient of thermal expansion (Landau & Lifshitz 1987, § 56).

When both the temperature gradient and gravitational acceleration $\boldsymbol{g}$ lie on the plane of the cell, the chiral velocity arising from the underbraced term in (6.9) is

$$v^{ch} \sim \chi\,\frac{R^3 \rho g \alpha_T\,\Delta T}{\eta d}. \tag{6.10}$$

This effect is present when the Rayleigh number exceeds its critical value. It is separate from the one discussed in the present paper, and will be analysed in detail elsewhere.

7. Discussion

Following the constitutive relations introduced in Andreev *et al.* (2010), but now with temperature-dependent material parameters, in this paper we developed a theory to calculate the thermally-induced chiral current $\boldsymbol{j}^{ch}$ in a suspension of n^+ right-handed and n^- left-handed chiral particles. The main result is the linear in ΔT expression for the chiral velocity v^{ch} established in (4.7), and its commensurate chiral current (3.1) in crossed temperature and pressure gradients, as displayed in figure 1. The chiral suspension applies stresses on the base liquid; cf. (3.9). These stresses, allowed by symmetry, endow the base flow with a component that is transverse to the direction of both the flow and the temperature gradient. As remarked by Witten & Diamant (2020, § 7.3) in reviewing Andreev *et al.* (2010), this behaviour resembles the Hall effect.

The main concepts developed in this paper can be traced back to the theory of non-centrosymmetric media (Sturman & Fridkin 2021). More recently, these ideas were employed in the photo-induced separation of chiral isomers (Spivak & Andreev 2009), the photo-galvanic effect (Deyo *et al.* 2009), the propulsion of chiral particles (Kirkinis *et al.* 2012) by taking advantage of their electric polarization and magnetic moment, and finally, passive propulsion and separation, taking advantage of the rotational degrees of freedom of the medium (Kirkinis & Olvera de la Cruz 2023).

Acknowledgements. We are grateful for comments and suggestions of two anonymous referees that significantly improved the manuscript.

Funding. We thank the Department of Energy, Office of Basic Energy Sciences for support under contract DE-FG02-08ER46539 and the Center for Computation & Theory of Soft Materials at Robert R. McCormick School of Engineering and Applied Science, Northwestern University (M.O.C. and E.K.). The work of A.V.A. was supported, in part, by the US National Science Foundation through the MRSEC grant no. DMR-1719797, the Thouless Institute for Quantum Matter, and the College of Arts & Sciences at the University of Washington.

Declaration of interests. The authors report no conflict of interest.

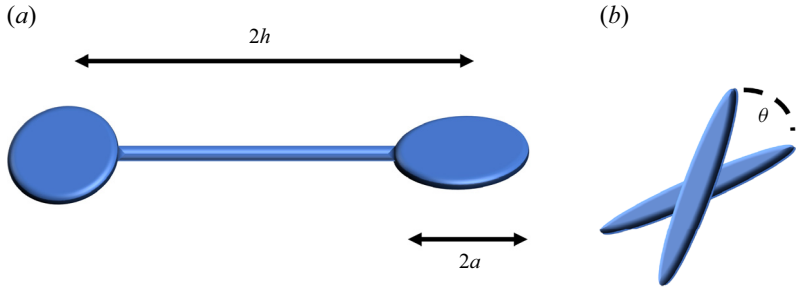

Figure 8. (*a*) Paddle-like chiral particle employed in the single-particle theory based on the resistance matrix formulation (Makino & Doi 2004, 2017). Centre-to-centre distance is $2h$, and the radius of each disk is a. We take the characteristic size of the paddle-like chiral particle to be $h \sim R$, according to the notation introduced in the present paper. (*b*) Definition of the angle θ employed in the mobility tensor to characterize the degree of chirality of a single particle (Makino & Doi 2017); see (A1).

Author ORCIDs.
E. Kirkinis https://orcid.org/0000-0002-1140-9632;
A.V. Andreev https://orcid.org/0000-0001-6340-6671;
M. Olvera de la Cruz https://orcid.org/0000-0002-9802-3627.

Appendix A. Particle shape dependence of the chirality parameter χ

In the Introduction (below (1.1)), we mentioned that χ is a geometric scalar coefficient characteristic of the particle shape and thus it should be described by an expression that vanishes for a non-chiral particle. For chiral particles of gradually varying chiral shape, it should change continuously. Below, we employ single-particle theory (Makino & Doi 2004, 2017) to obtain such a qualitative expression.

The drift particle velocity in a linear shear flow has the form $\boldsymbol{V}^{sp} = \tilde{g}\boldsymbol{E}$ (cf. Makino & Doi 2004, 2017), where the superscript 'sp' stands for 'single particle' (theory), $\tilde{g}$ is the third rank mobility tensor, and $\boldsymbol{E}$ is the rate-of-strain tensor of the flow. For a paddle-like particle as displayed in figure 8, the form of the third rank tensor $\tilde{g}$ was derived in closed form in the aforementioned references. Its coefficients $g(a, h; \theta)$ in the particle frame of reference, which are homogeneous functions of degree 1 (in the variables a and h), can be written succinctly in the form (Makino & Doi 2017, (27))

$$g(a, h; \theta) = -\frac{a^2 h\,(\sin(2\theta) \pm 2\sin(\theta))}{8a^2\cos(\theta) \pm 40a^2 \pm 48h^2}, \tag{A1}$$

where θ is the angle formed between the two blades as depicted in figure 8(*b*). Thus the angle $\theta = 0$ corresponds to a non-chiral particle, and there are angles where g reaches a maximum, which we employ here to characterize what is meant by the phrase 'strong chirality'. Note that the drift velocity $\boldsymbol{V}^{sp}$ generates a back-flow in the liquid and a commensurate shear stress (Witten & Diamant 2020, § 7.3) proportional to

$$\frac{V^{sp}}{d} \sim g(a, h; \theta)\,\frac{U_0}{d^2}. \tag{A2}$$

We show below that χ is proportional to g in (A1). Consider a non-racemic chiral suspension characterized by the chiral stress (3.9). It is proportional to $n^{ch}\alpha\,\partial_y^2 u$. Considering the scaling forms $n^{ch} \sim R^{-3}$ and $\alpha \sim \chi R^4$, introduced in the main body of the

paper, we obtain the chiral shear stress to be proportional to $\chi R(U_0/d^2)$. Comparison with (A2) leads to the conclusion that $\chi \propto \hat{g}(\theta)$, where $\hat{g}(\theta)$ is the dimensionless counterpart of coefficient (A1), whose length scale dimension has been factorized (this is possible because g is a homogeneous function of a and h of degree 1). Thus χ vanishes for a non-chiral paddle-like particle of the type displayed in figure 8 (for $\theta = 0$), and it can acquire finite values for strongly chiral shapes.

Single-particle theory, as described above, provides an estimate for the tensor $\hat{g}(\theta)$ to be of the order of 0.03 for strongly chiral particles. On the other hand, in this paper, which is based on the continuum theory, we have set $\chi = O(1)$ in evaluating the various observables. This is a rough estimate for strongly chiral particles that were shown in Kirkinis & Olvera de la Cruz (2023) to generate chiral forces of the same order of magnitude as those occurring in comparable-size systems employed in technology and biology; cf. Kataoka & Troian (1999) and Ando & Yamamoto (2009).

References

Ando, J. & Yamamoto, K. 2009 Vascular mechanobiology endothelial cell responses to fluid shear stress. *Circ. J.* **73** (11), 1983–1992.

Andreev, A.V., Son, D.T. & Spivak, B. 2010 Hydrodynamics of liquids of chiral molecules and suspensions containing chiral particles. *Phys. Rev. Lett.* **104** (19), 198301.

Arnold, M.S., Green, A.A., Hulvat, J.F., Stupp, S.I. & Hersam, M.C. 2006 Sorting carbon nanotubes by electronic structure using density differentiation. *Nat. Nanotechnol.* **1** (1), 60–65.

Chandrasekhar, S. 1961 *Hydrodynamic and Hydromagnetic Stability*. Oxford University Press.

Datt, C. & Elfring, G.J. 2019 Active particles in viscosity gradients. *Phys. Rev. Lett.* **123** (15), 158006.

Davis, S.H., Kriegsmann, G.A., Laurence, R.L. & Rosenblat, S. 1983 Multiple solutions and hysteresis in steady parallel viscous flows. *Phys. Fluids* **26** (5), 1177–1182.

Deyo, E., Golub, L.E., Ivchenko, E.L. & Spivak, B. 2009 Semiclassical theory of the photogalvanic effect in non-centrosymmetric systems. arXiv:0904.1917.

Ehrhard, P. 1993 Experiments on isothermal and non-isothermal spreading. *J. Fluid Mech.* **257**, 463–483.

Fan, J., Zhang, H., Rahman, T., Stanton, D.N. & Wan, L.Q. 2019 Cell organelle-based analysis of cell chirality. *Commun. Integr. Biol.* **12** (1), 78–81.

Fogel'son, R.L. & Likhachev, E.R. 2001 Temperature dependence of viscosity. *Tech. Phys.* **46** (8), 1056–1059.

Gao, C., Kewalramani, S., Valencia, D.M., Li, H., McCourt, J.M., Olvera de la Cruz, M. & Bedzyk, M.J. 2019 Electrostatic shape control of a charged molecular membrane from ribbon to scroll. *Proc. Natl Acad. Sci. USA* **116** (44), 22030–22036.

Gavis, J. & Laurence, R.L. 1968 Viscous heating in plane and circular flow between moving surfaces. *Ind. Engng Chem. Fundam.* **7** (2), 232–239.

Happel, J. & Brenner, H. 1965 *Low Reynolds Number Hydrodynamics with Special Applications to Particulate Media*. Prentice-Hall.

Inaki, M., Liu, J. & Matsuno, K. 2016 Cell chirality: its origin and roles in left–right asymmetric development. *Phil. Trans. R. Soc. Lond.* B **371** (1710), 20150403.

Kataoka, D.E. & Troian, S.M. 1999 Patterning liquid flow on the microscopic scale. *Nature* **402** (6763), 794–797.

Kirkinis, E. & Andreev, A.V. 2019 Healing of thermocapillary film rupture by viscous heating. *J. Fluid Mech.* **872**, 308–326.

Kirkinis, E., Andreev, A.V. & Spivak, B. 2012 Electromagnetic propulsion and separation by chirality of nanoparticles in liquids. *Phys. Rev.* E **85**, 016321.

Kirkinis, E. & Olvera de la Cruz, M. 2023 Activity-induced separation of passive chiral particles in liquids. *Phys. Rev. Fluids* **8** (2), 023302.

Landau, L.D. & Lifshitz, E.M. 1987 *Fluid Mechanics*. Course of Theoretical Physics, vol. 6. Pergamon.

Makino, M. & Doi, M. 2004 Brownian motion of a particle of general shape in Newtonian fluid. *J. Phys. Soc. Japan* **73** (10), 2739–2745.

Makino, M. & Doi, M. 2017 Separation of propeller-like particles by shear and electric field. *Phys. Rev. Fluids* **2** (6), 064303.

McCourt, J.M., Kewalramani, S., Gao, C., Roth, E.W., Weigand, S.J., Olvera de la Cruz, M. & Bedzyk, M.J. 2022 Electrostatic control of shape selection and nanoscale structure in chiral molecular assemblies. *ACS Cent. Sci.* **8** (8), 1169–1181.

Nagarsekar, K., Ashtikar, M., Steiniger, F., Thamm, J., Schacher, F. & Fahr, A. 2016 Understanding cochleate formation: insights into structural development. *Soft Matt.* **12** (16), 3797–3809.

Oda, R., Huc, I., Schmutz, M., Candau, S.J. & MacKintosh, F.C. 1999 Tuning bilayer twist using chiral counterions. *Nature* **399** (6736), 566–569.

Oppenheimer, N., Navardi, S. & Stone, H.A. 2016 Motion of a hot particle in viscous fluids. *Phys. Rev. Fluids* **1** (1), 014001.

Potter, M.C. & Graber, E. 1972 Stability of plane Poiseuille flow with heat transfer. *Phys. Fluids* **15** (3), 387–391.

Schermer, R.T., Olson, C.C., Coleman, J.P. & Bucholtz, F. 2011 Laser-induced thermophoresis of individual particles in a viscous liquid. *Opt. Express* **19** (11), 10571–10586.

Shimizu, T., Masuda, M. & Minamikawa, H. 2005 Supramolecular nanotube architectures based on amphiphilic molecules. *Chem. Rev.* **105** (4), 1401–1444.

Shoele, K. & Eastham, P.S. 2018 Effects of nonuniform viscosity on ciliary locomotion. *Phys. Rev. Fluids* **3** (4), 043101.

Spivak, B. & Andreev, A.V. 2009 Photoinduced separation of chiral isomers in a classical buffer gas. *Phys. Rev. Lett.* **102** (6), 063004.

Sturman, B.I. & Fridkin, V.M. 2021 *The Photovoltaic and Photorefractive Effects in Noncentrosymmetric Materials*. Routledge.

Sukanek, P.C., Goldstein, C.A. & Laurence, R.L. 1973 The stability of plane Couette flow with viscous heating. *J. Fluid Mech.* **57** (4), 651–670.

Wall, D.P. & Wilson, S.K. 1996 The linear stability of channel flow of fluid with temperature-dependent viscosity. *J. Fluid Mech.* **323**, 107–132.

Witten, T.A. & Diamant, H. 2020 A review of shaped colloidal particles in fluids: anisotropy and chirality. *Rep. Prog. Phys.* **83** (11), 116601.

Zhang, H., Duan, W., Lu, M., Zhao, X., Shklyaev, S., Liu, L., Huang, T.J. & Sen, A. 2014 Self-powered glucose-responsive micropumps. *ACS Nano* **8** (8), 8537–8542.